doi:10.1093/brain/awx377 BRAIN 2018: 141; 651–661 | 651

BRAIN
A JOURNAL OF NEUROLOGY

REPORT

A homozygous *ATAD1* mutation impairs postsynaptic AMPA receptor trafficking and causes a lethal encephalopathy

Juliette Piard,[1,2,*] George K. Essien Umanah,[3,4,*] Frederike L. Harms,[5,*] Leire Abalde-Atristain,[3,6] Daniel Amram,[7] Melissa Chang,[3,4] Rong Chen,[3,4] Malik Alawi,[8,9] Vincenzo Salpietro,[10] Mark I. Rees,[11] Seo-Kyung Chung,[11] Henry Houlden,[10] Alain Verloes,[12] Ted M. Dawson,[3,4,6,13,14] Valina L. Dawson,[3,4,6,13,15,#] Lionel Van Maldergem[1,2,16,#] and Kerstin Kutsche[5,#]

[*,#]These authors contributed equally to this work.

Members of the AAA+ superfamily of ATPases are involved in the unfolding of proteins and disassembly of protein complexes and aggregates. *ATAD1* encoding the ATPase family, AAA+ domain containing 1-protein Thorase plays an important role in the function and integrity of mitochondria and peroxisomes. Postsynaptically, Thorase controls the internalization of excitatory, glutamatergic AMPA receptors by disassembling complexes between the AMPA receptor-binding protein, GRIP1, and the AMPA receptor subunit GluA2. Using whole-exome sequencing, we identified a homozygous frameshift mutation in the last exon of *ATAD1* [c.1070_1071delAT; p.(His357Argfs*15)] in three siblings who presented with a severe, lethal encephalopathy associated with stiffness and arthrogryposis. Biochemical and cellular analyses show that the C-terminal end of Thorase mutant gained a novel function that strongly impacts its oligomeric state, reduces stability or expression of a set of Golgi, peroxisomal and mitochondrial proteins and affects disassembly of GluA2 and Thorase oligomer complexes. *Atad1*$^{-/-}$ neurons expressing Thorase mutant^{His357Argfs*15} display reduced amount of GluA2 at the cell surface suggesting that the Thorase mutant may inhibit the recycling back and/or reinsertion of AMPA receptors to the plasma membrane. Taken together, our molecular and functional analyses identify an activating *ATAD1* mutation as a new cause of severe encephalopathy and congenital stiffness.

1 Centre de génétique humaine, Université de Franche-Comté, Besançon, France
2 Integrative and Cognitive Neurosciences Research Unit EA481, University of Franche-Comté, Besançon, France
3 Neuroregeneration and Stem Cell Programs, Institute for Cell Engineering, Johns Hopkins University School of Medicine, Baltimore, MD 21205, USA
4 Department of Neurology, Johns Hopkins University School of Medicine, Baltimore, MD 21205, USA
5 Institute of Human Genetics, University Medical Center Hamburg-Eppendorf, 20246 Hamburg, Germany
6 Cellular and Molecular Medicine Graduate Program, Johns Hopkins University School of Medicine, Baltimore, MD 21205, USA
7 Unité fonctionnelle de génétique clinique, Centre hospitalier intercommunal, Créteil, France
8 University Medical Center Hamburg-Eppendorf, Bioinformatics Core Facility, 20246 Hamburg, Germany
9 Heinrich-Pette-Institute, Leibniz-Institute for Experimental Virology, Virus Genomics, Hamburg, Germany
10 Department of Molecular Neuroscience, UCL Institute of Neurology, London, UK
11 Neurology Research Group, Institute of Life Science, Swansea University Medical School, Swansea University, Swansea, UK
12 Department of Genetics, Robert-Debré Hospital, Paris, France
13 Solomon H. Snyder Department of Neuroscience, Johns Hopkins University School of Medicine, Baltimore, MD 21205, USA

Received September 25, 2017. Revised November 20, 2017. Accepted November 27, 2017. Advance Access publication January 30, 2018

14 Department of Pharmacology and Molecular Sciences, Johns Hopkins University School of Medicine, Baltimore, MD 21205, USA
15 Department of Physiology, Johns Hopkins University School of Medicine, Baltimore, MD 21205, USA
16 Clinical Investigation Center 1431, National Institute of Health and Medical Research (INSERM), University of Franche-Comté, Besançon, France

Correspondence to: L. Van Maldergem, MD, PhD
Centre de génétique humaine
Université de Franche-Comté
Centre Hospitalier Universitaire
2 place St Jacques
25000 Besancon
France
E-mail: lionel.van-maldergem@inserm.fr

Keywords: *ATAD1*; encephalopathy; AMPA receptor trafficking
Abbreviation: AMPAR = AMPA receptor

Introduction

Early-infantile onset encephalopathies come with an urgent need for a proper diagnosis as immediate therapeutic decisions have to be made. The majority of these disorders have a genetic aetiology and follow a Mendelian inheritance pattern. Thus, whole-exome sequencing is the method of choice to elucidate the related gene in extremely rare forms of early-onset encephalopathies that can lead to early death (Cartault *et al.*, 2012; Kevelam *et al.*, 2013).

The AAA+ family is a large enzymatic group of ATPases associated with various cellular activities that induce conformational changes in a wide range of substrate proteins. These ATPases have been involved in various human diseases such as peroxisome biogenesis disorders, early-onset torsion dystonia linked to *DYT1*, *SPG4*- and *SPG7*-related hereditary spastic paraplegia and a specific form of inclusion body myopathy (Hanson and Whiteheart, 2005). One of them, the AAA+ ATPase Thorase encoded by *ATAD1* plays a critical role in regulating the surface-expression of AMPA receptors (alpha-amino-3-hydroxy-5-methylisoxazole-4-proprionate receptors), thus regulating synaptic plasticity, learning and memory (Ahrens-Nicklas *et al.*, 2017). Here, we report the genotype–phenotype relationship in three infants exhibiting a severe lethal encephalopathy with neonatal stiffness and arthrogryposis resulting from a homozygous activating *ATAD1* mutation.

Material and methods

Exome sequencing and sequence data analysis

Written informed consent was received from participants prior to inclusion in the study. Targeted enrichment and massively parallel sequencing were performed on genomic DNA. Enrichment of the whole exome was performed according to the manufacturer's protocols using the Nextera Enrichment Kit (62 Mb) (Illumina) for Patients 1 and 2 and their mother (Kortüm *et al.*, 2015). Captured libraries were then loaded onto the 2500 platform (Illumina). Trimmomatic was used to remove adapters, low quality (phred quality score < 5) bases from the 3′ ends of sequence reads (Bolger *et al.*, 2014). Reads shorter than 36 bp were subsequently removed. Further processing was performed following the Genome Analysis Toolkit's (GATK) best practice recommendations. Briefly, trimmed reads were aligned to the human reference genome (UCSC GRCh37/hg19) using the Burrows-Wheeler Aligner (BWA mem v0.7.12). Duplicate reads were marked with Picard tools (v1.141). GATK (v3.4) was used for indel realignment, base quality score recalibration, calling variants using the HaplotypeCaller, joint genotyping, and variant quality score recalibration. AnnoVar (v2015-03-22) was used to functionally annotate and filter alterations against public databases (dbSNP138, 1000 Genomes Project, and ExAC Browser). Exonic variants and intronic alterations at exon–intron boundaries ranging from −10 to +10, which were clinically associated and with allele frequencies $<0.5\%$ without homozygous carriers in public databases, were retained.

Variant validation

Sequence validation and segregation analysis for all candidate variants were performed by Sanger-sequencing. Primer pairs designed to amplify selected coding exons and exon–intron boundaries of candidate genes and PCR conditions are available on request. Amplicons were directly sequenced using the ABI BigDye™ Terminator Sequencing Kit (Applied Biosystems) and an automated capillary sequencer (ABI 3500; Applied Biosystems). Sequence electropherograms were analysed using the Sequence Pilot SeqPatient software (JSI medical systems).

RNA isolation, cDNA synthesis and sequencing

Total RNA was extracted (RNeasy® Mini kit, Qiagen) from cultured primary fibroblasts obtained from Patient 1 and a control individual. One microgram of total RNA was reverse transcribed (Superscript™ III RT, Thermo Fisher) using random hexamers as primers, and 1 µl of the reverse transcription reaction was used to amplify a 669-bp *ATAD1* cDNA fragment encompassing the c.1070_1701delAT variant (forward primer 5′-ATGATGAAAGCTCAGTTTATGAGTC-3′, reverse primer 5′-GGAACAGTTGAATCCAGCCT-3′). The PCR product was directly sequenced.

Antibodies and plasmids

All antibodies were acquired commercially: Thorase (mAb, Neuromab, RRID: AB_2564836), GluA2-N/C (mAb, Millipore-Chemicon, RRID: AB_2113875 and RRID: AB_2247874) and GRIP1 (pAb, Millipore-Chemicon, RRID: AB_11210079), Tomm20, Cox 4, Hexokinase 1, GOS28, PEX26 and VDAC1 (Cell Signaling), actin-HRP were purchased from GE healthcare (Amersham). *N*-methyl-D-aspartate (NMDA) was purchased from Sigma-Aldrich. Plasmids are described in the 'Recombinant protein expression and ATPase activity assays' section.

Protein expression and measurement of oxygen consumption rate in patient cells

Patient-derived and control fibroblast cells were maintained in Dulbecco's modified Eagle medium (DMEM, Corning Cellgro) plus 10% (v/v) foetal bovine serum (FBS) and 1% (v/v) Penicillin-Streptomycin (Corning Cellgro), at 37°C with a 5% CO_2 atmosphere in a humidified incubator. Thorase expression and comparative immunoblot analyses were performed using cell lysates from patient and control fibroblasts. Protein concentrations were determined by BCA protein assay (Pierce™, Thermo Scientific) and 20 µg were resolved on SDS-PAGE. The immunoblot membranes were stained with Ponceau stain to assess loading of proteins. Immunoblot analyses were performed using antibodies to COX4, Hexokinase 1 (HXK1), PEX26, VDAC1 and actin (GE Healthcare) as control for loading. Band intensities were quantified using ImageJ (NIH) and normalized to actin. The values obtained from ImageJ were further analysed to determine significant differences using GraphPad Prism software (GraphPad).

The patient-derived and control fibroblast cells cultured on glass coverslips were fixed by replacing the media with phosphate-buffered saline (PBS) containing 4% paraformaldehyde and incubated for 10 min. The cells were washed three times with PBS and then were permeabilized with 0.5% Triton™ X-100 in blocking buffer (5% goat serum in PBS) for 30 mins. The blocking buffer was replaced with PBS containing Tomm20, GOS28 or PEX26 antibodies (1:1000 dilution) at 4°C overnight. Cells were washed three times with PBS, and incubated with fluorescent secondary antibodies (Alexa Fluor® 488, Life Technologies) for 2 h. Coverslips were washed twice followed by 5 min incubation with PBS containing DAPI to stain the nuclei and then washed three times with PBS. The coverslips were mounted on glass slides with Immu-Mount™ (Thermo Scientific) and imaged using Zeiss LSM Confocal microscope.

Mitochondrial oxygen consumption rate (OCR) was assessed in patient-derived and control fibroblast cells in an XF24 Extracellular Flux Analyzer (Seahorse Bioscience), as described previously (Chen *et al.*, 2014). Fibroblast cells ($\sim 0.5 \times 10^6$ per well) culture media was replaced with XF24 DMEM containing 10 mM glucose, 2 mM L-glutamine (Life Technologies) and 2 mM sodium pyruvate (Life Technologies). OCR was measured at 37°C with 1-min mix, 1-min wait, and 5-min measurement. The OCR was then analysed in the presence of oligomycin, carbonilcyanide m-cholorophenylhydrazone (CCCP) and rotenone after 30 min incubation in a CO_2-free incubator to assess coupling of respiratory chain and mitochondrial respiratory capacity. The OCRs were normalized relative to cell number and basal respiration in each well and is presented as per cent change. The significant differences in values obtained were analysed using GraphPad Prism software (GraphPad).

3D structure modelling

The C-termini of Thorase wild-type (Gln259-Asp361) and mutant^{His357Argfs*15} (Gln259-Gln370) were modelled using the SWISS-MODEL (Arnold *et al.*, 2006) and confirmed by Phyre2 (Kelley *et al.*, 2015) protein modelling, prediction and analysis software. All images obtained were viewed and labelled with pdb viewer, Pymol. The 3D models are shown as obtained from the SWISS-MODEL software without any modification.

Recombinant protein expression and ATPase activity assays

GST-Thorase was generated by cloning the coding sequence of *ATAD1* wild-type or mutant^{His357Argfs*15} into pGEX6P1 (GE Healthcare) between *Bam*HI and *Xho*I. Thorase wild-type or mutant^{His357Argfs*15} coding sequence were also cloned into FUGW (Adgene) between *Age*I and *Bam*HI to generate GFP-tagged Thorase. GST-tagged fusion proteins were expressed in *Escherichia coli* strain BL21-CodonPlus (DE3)-RIPL (Stratagene) and purified by using GSTrap (GE Healthcare), respectively following the manufacturer's instructions. To obtain non-tagged Thorase proteins, GST-Thorase bound to beads were treated with PreScission protease (GE Healthcare) to cleave Thorase from GST. The eluted Thorase was further purified by

size exclusion chromatography using Superdex 200 10/300GL column (GE Healthcare). The purity of the recombinant proteins was assessed by SDS-PAGE followed by Coomassie blue staining. Immunoblotting was used to confirm the presence of proteins in the purified samples.

The ATPase activities of Thorase wild-type and mutant^{His357Argfs*15} were assessed by measuring ATP hydrolysis and [α-^{32}P]-ATP binding. ATP hydrolysis measurements were carried out using an ADP colorimetric assay kit (BioVision) according to the instructions from the manufacturer. Approximately 1 mg of purified non-tagged Thorase recombinant proteins were incubated with 20, 40, 60, 80, 100 and 120 μM ATP in 0.5 ml of ADP assay buffer (supplemented with 2 mM $MgCl_2$) at 37°C for 30 min. The amount of ADP formed due to ATP hydrolysis was then determined to assess the ATPase activity of Thorase mutant^{His357Argfs*15} compared to wild-type. The ATP binding was evaluated by a photo-labelling technique as described by Babst *et al.* (1998). Approximately 2.0 mg of purified non-tagged Thorase proteins in 0.1 ml nucleotide binding buffer (50 mM Tris.Cl pH 7.5, 150 mM NaCl, 2 mM $MgCl_2$, 5% glycerol) containing 0.1 mM [α-^{32}P]ATP were incubated at 4°C for 1 h. The mixtures were exposed to UV light to cross-link the bound [α-^{32}P]ATP to Thorase, and SDS-PAGE sample buffer was added to stop the reaction. The samples were resolved on SDS-PAGE, and then exposed to a phosphor screen (Perkin Elmer). A scanning densitometer was used to quantify the amount of ^{32}P protein labelling in the samples.

GST-Thorase pull-down of GluA2-GRIP1 complex

For the pull-down assay, purified GST-tagged Thorase proteins immobilized on glutathione Sepharose® beads were incubated with 1 mg of *Atad1* knockout whole brain lysates (homogenized in nucleotide binding buffer with 1% Triton™ X-100) in the presence of 2 mM ADP, ATP or non-hydrolysable ATPγS for 2 h at 4°C followed by 30 min at 37°C. The beads were thoroughly washed four times and the bound proteins were eluted in SDS-PAGE sample loading buffer followed by immunoblot analysis with mouse anti-Thorase, anti-GluA2 and anti-GRIP1 antibodies.

Thorase oligomer assembling and disassembling assays

Thorase mutant^{His357Argfs*15} oligomer formation was evaluated by chemical cross-linking using glutaraldehyde as previously described (Babst *et al.*, 1998). Approximately 1.0 mg purified Thorase proteins in nucleotide binding buffer with 2 mM ATP or non-hydrolysable ATPγS were incubated at 4°C for 2 h (to allow oligomer assembling) followed by incubation at 37°C for 30 min (to allow oligomer disassembling). The cross-linking reaction was stopped by addition of glycine to a final concentration of 10 mM and samples were mixed with SDS-PAGE sample loading buffer. The samples were resolved on 4–20% gradient SDS-PAGE (Invitrogen) and immunoblotted with anti-Thorase antibody to evaluate the presence of Thorase oligomer complex.

Surface expression and NMDA-induced endocytosis of GluA2 assays

The effects of the *ATAD1* mutation p.(His357Argfs*15) on GluA2 (encoded by *GRIA2*) surface expression were examined in primary cortical neuron cultures prepared from embryonic Day 15 embryos obtained from heterozygous (*Atad1*$^{+/-}$ × *Atad1*$^{+/-}$) breeding as previously described (Zhang *et al.*, 2011; Prendergast *et al.*, 2014). The neurons were infected with Thorase-GFP viruses 12 days after plating. To estimate surface GluA2 surface expression in non-treated (control) and NMDA-induced endocytosis, live neurons were incubated with 2 mg of mouse-monoclonal anti-N-terminal GluA2 antibodies at 37°C for 1 h in neuronal growth media. The neurons were washed twice with fresh growth medium and then replaced with media containing Tyrodes' buffer (119 mM NaCl, 5 mM KCl, 25 mM HEPES, 2 mM $CaCl_2$, 2 mM $MgCl_2$, 1 μM TTX + 100 μM LY34195) with 20 μM CNQX followed by treatment with or without 100 μM NMDA for 5 min at 37°C in Tyrodes' buffer containing 300 μM $MgCl_2$ and 10 μM glycine. The media was replaced with 4% paraformaldehyde and 4% sucrose in PBS for 15 min to fix the neurons. The neurons were washed three times with PBS followed by treatment with 5% goat serum, 0.3% Triton™ X-100 in PBS for 1 h at 4°C and overnight incubation with rabbit-monoclonal anti-C-terminal GluA2 antibody. The neurons were incubated with mouse Alexa Fluor® 555-conjugated and rabbit Alexa Fluor® 350-conjugated secondary antibodies (Invitrogen) for 2 h after three washes with PBS followed by three washes with PBS before imaging. Images were acquired by using a Zeiss LSM 710 laser-scanning confocal microscope. The fluorescence intensities were measured and the internalization index was calculated by intracellular fluorescence divided by total fluorescence normalized to untreated neurons.

AMPA receptor (AMPAR) surface expression was also evaluated using surface protein-crosslinking assay. Primary cortical neuron cultures infected with Thorase-GFP viruses were treated with/without NMDA as described above (Zhang *et al.*, 2011; Prendergast *et al.*, 2014). Immediately after NMDA treatment the medium was replaced with ice-cold artificial CSF containing 2 mM membrane-impermeant crosslinking agents, bis(sulphosuccinimidyl)-suberate [BS3, (Pierce Biotechnology)] (Conrad *et al.*, 2008) to selectively crosslink cell surface proteins for 30 min. The reaction was quenched by replacing the BS3 solution with artificial CSF containing 0.1 M glycine (with 10 mins incubation) followed by three washes with artificial CSF containing 0.1 M glycine.

The neurons were suspended in lysis buffer (nucleotide binding buffer with 1% Triton™ X-100, and protease inhibitors) and the total protein concentrations were determined. Equal amount of proteins were resuspended in SDS-PAGE loading buffer, resolved on 4–12% gradient SDS-PAGE and western immunoblotting was performed to analyse the surface and intracellular pools of AMPA receptors using anti-GluA2 and anti-Thorase antibodies.

Data analyses and statistics

All experiments were repeated at least three times and quantitative data are presented as the mean ± standard error of the mean (SEM) performed by GraphPad prism6 software (Instat, GraphPad Software). Statistical significance was assessed by one-way ANOVA. The significant differences were identified by *post hoc* analysis using the Tukey-Kramer *post hoc* method for multiple comparisons. Assessments were considered significant with $P < 0.05$. Power analysis and sample size calculation for all experiments were determined using G*Power 3.1 statistics software.

Results

Three siblings with severe encephalopathy and a homozygous *ATAD1* mutation

The three siblings were born at term by caesarean section for foeto-pelvic disproportion with normal growth parameters. Pregnancies were marked by maternal diabetes. Healthy parents are first cousins and originated from southern Tunisia. The first patient (Patient 1; IV:1; Fig. 1A) was a male who presented at birth with respiratory distress requiring assisted ventilation. Generalized hypertonia with an exaggerated startle reflex, adducted thumbs, spontaneous tremor and clonic movements were observed from Day 1. EEG showed altered background with slow and disorganized activity and multiple multifocal epileptic discharges. Examination at 2 months showed major stiffness and distal arthrogryposis with fixed prone position of upper limbs and bilateral camptodactyly. Deep tendon reflexes were brisk with extensor plantar reflex. Visual contact was absent and narrow miosis unresponsive to light was noted. Facial distinctive features including inexpressive facies, anteverted nares, high arched palate and brachycephaly were observed. Kyphoscoliosis and benign umbilical hernia were also noted. He had several episodes of pneumonia and died after multiple organ failure at the age of 5 months. Abdominal ultrasound, eye fundus, spinal cord and brain MRI were normal. Skeletal X-rays indicated dorsal scoliosis. A large metabolic screening and array CGH did not show any abnormality. A muscle biopsy was performed and showed focal atrophy of both fibre types with grouping suggesting an underlying neurogenic disorder. His younger brother (Patient 2; IV:2; Fig. 1A) presented at birth with respiratory distress, poor spontaneous mobility and no visual contact. Examination showed generalized hypertonia with transient tremor, bilateral adducted thumbs and clenched toes. He underwent surgery for bilateral inguinal hernia at 2 months. Regular

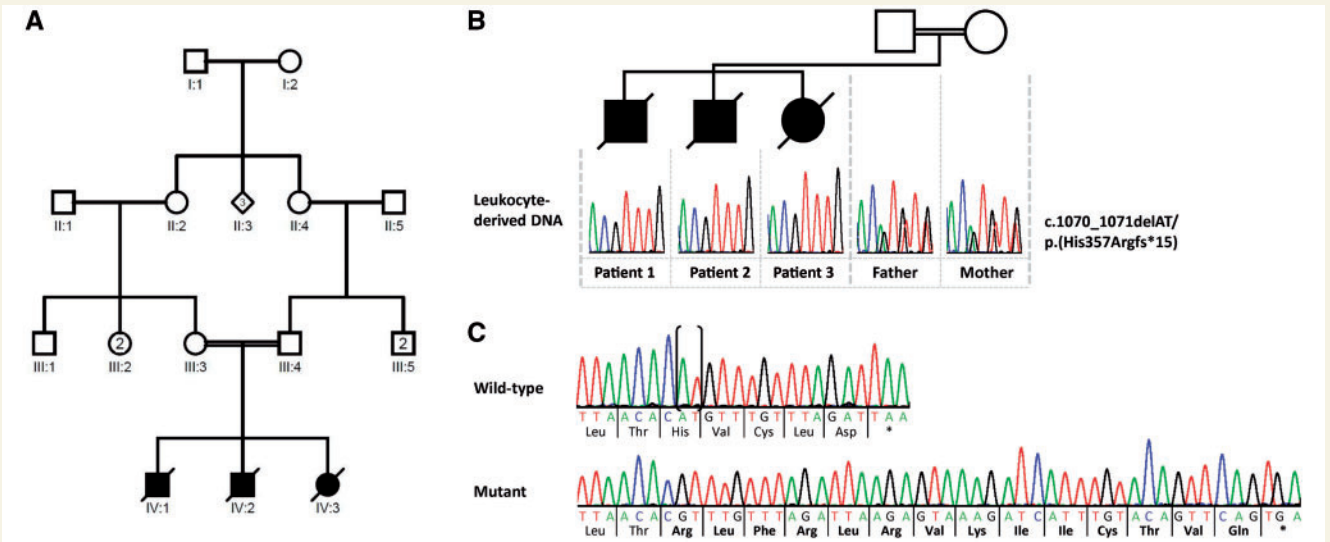

Figure 1 DNA and RNA analysis in the family with three siblings carrying the homozygous *ATAD1* mutation. (**A**) Pedigree of the family. (**B**) Partial sequence electropherograms demonstrating the *ATAD1* c.1070_1071delAT [p.(His357Argfs*15)] mutation in the homozygous state in leucocyte-derived DNA of the affected siblings (Patients 1–3). Their healthy parents (father and mother) are heterozygous carriers of the mutation. (**C**) Partial sequence electropherograms show the 2-bp deletion in *ATAD1* in fibroblast-derived cDNA of one sibling (Mutant) in comparison to the cDNA sequence of a healthy individual (Wild-type). Deleted bases are marked by parenthesis in the normal sequence. The encoded amino acid residues are depicted below each sequence in the three-letter code and show the 14 novel amino acid residues at the C-terminus of ATAD1 (highlighted in bold). Asterisk indicates a stop codon.

swallowing difficulties resulted in food misrouting accidents with subsequent pneumonia. In contrast to his brother, a few intentional smiles were noted before death, after a novel episode of aspiration pneumonia at the age of 3 months. The ultrasound follow-up of the third pregnancy indicated decreased foetal movements during the third trimester. The girl (Patient 3; IV:3; Fig. 1A) presented at birth with transient respiratory distress requiring assisted ventilation. In her case, axial hypotonia contrasted with limb hypertonia. Examination showed poor spontaneous mobility, distal arthrogryposis with adducted thumbs, ulnar deviation and bilateral clubfoot. Eye contact was present. She had gastro-oesophageal reflux. Brain MRI performed at Day 1 showed myelination delay and a periventricular white matter hypersignal. EEGs were normal. She died at the age of 6 months. The common clinical features of the siblings can be summarized as onset of rigidity at birth, no achievement of developmental milestones and death within the first months of life. Array CGH and Sanger-sequencing of *GLRA1* and *SLC6A5* mutated in hyperekplexia (Tijssen and Rees, 1993; Carta *et al.*, 2012) and *SCN4A* mutated in congenital paramyotonia (Koch *et al.*, 1991) did not identify any molecular alteration in the oldest sibling (Patient 1) (data not shown). The severe encephalopathy in the index patient remained thus unexplained. Next, we performed whole-exome sequencing in two affected siblings (Patients 1/IV:1 and 3/IV:3) and their healthy mother (Patient III:3; Fig. 1A and B). Given parental consanguinity, analysis of whole-exome sequencing data was performed according to an autosomal recessive inheritance model. We identified five rare homozygous variants [with an allele frequency $<0.5\%$ in population databases (dbSNP138, 1000 Genomes Project, Exome Variant Server, ExAC and gnomAD browsers) and no homozygous carriers in the ExAC and gnomAD browsers] shared by the two affected siblings and present in the heterozygous state in their healthy mother (Supplementary Table 1). Segregation analysis excluded two of the variants (Supplementary Table 2), while the remaining variants in *RNLS*, *CDH8* and *ATAD1* are not located within a region of significant homozygosity as assessed by homozygosity mapper (Seelow *et al.*, 2009). However, *RNLS* and *ATAD1* are located in a homozygous region of ~1.3 Mb on chromosome 10 (data not shown). *In silico* pathogenicity assessment and splice-site tools predicted no deleterious effect on protein function for the missense variant p.(Ile114Val) in *RNLS* (Supplementary Table 3) and no pre-mRNA splicing alteration for the synonymous variant c.726T>C in *CDH8* (Supplementary Table 4). In contrast, the 2-bp deletion c.1070_1071delAT in the last exon of *ATAD1* was predicted to result in a frameshift with deletion of five amino acids and addition of 14 unrelated ATAD1 residues at the C-terminus [p.(His357Argfs*15)], possibly altering protein function (Fig. 1C, Supplementary Table 3 and Supplementary Fig. 1). The c.1070_1071delAT variant represents a very rare *ATAD1* allele, as it has an allele frequency of 0.00001221 in the gnomAD browser (three heterozygotes in 245 646 alleles; Supplementary Table 1), in accordance with the rarity of the signs and symptoms presented in the three siblings. *ATAD1* mRNA analysis from patient-derived fibroblasts demonstrated the presence of transcripts harbouring the −2 frameshift at codon 357 and 14 novel codons followed by the stop codon TGA at the 3′ end (Fig. 1C). These data indicate that mutated *ATAD1* mRNAs escape nonsense-mediated mRNA decay.

To identify additional *ATAD1* variants in individuals with a phenotype similar to that of the three siblings, two different patient cohorts were studied. First, we analysed whole-exome sequencing datasets of 2000 patients with epileptic encephalopathies and hereditary hyperekplexia. Second, 27 cases of glycinergic-negative hyperekplexia with parental consanguinity or atypical degenerative phenotype with severe developmental outcomes were screened by Sanger-sequencing. No further deleterious variant in *ATAD1* emerged from either datasets (data not shown), suggesting that *ATAD1*-related congenital encephalopathy with hypertonic stiffness is an extremely rare condition.

Altered protein levels but functional mitochondria in fibroblasts from a patient with the *ATAD1* mutation p.(His357Argfs*15)

ATAD1 mRNA analysis from patient-derived fibroblasts suggested that the mutated *ATAD1* mRNAs produce a protein with an altered C-terminal end. We examined the amount of ATAD1 protein in patient fibroblasts via immunoblotting, which confirmed that the C-terminally altered ATAD1 mutant is expressed in the patient cells (Fig. 2). Previous studies showed that the deletion of *ATAD1* causes accumulation of peroxisomal biogenesis factor 26 (PEX26) and Golgi SNARE 28 kDa (GOS28) in human cell lines (Chen *et al.*, 2014). In patient cells expressing mutant Thorase, protein level of PEX26 was slightly lower compared to control cells (Fig. 3A and B), however, we noticed variable expression of this and other proteins in control fibroblast cells (Fig. 3A and B). In addition, cytochrome *c* oxidase subunit 4 (COX4), hexokinase 1 (HXK1), and voltage-dependent anion channel 1 (VDAC1) were also reduced in patient fibroblasts (Fig. 3A and B). Staining of patient and control cells for GOS28 and PEX26 to evaluate the distribution of Golgi and peroxisomal proteins, respectively, showed that their levels were decreased in patient cells when compared to healthy controls (Fig. 3C). Thus, the frameshift mutation in *ATAD1* affects the stability or expression of GOS28 and PEX26. Interestingly, patient fibroblasts exhibited normal tubular mitochondrial morphology when stained for the mitochondrial protein TOMM20 (Fig. 3C). The patient fibroblasts also exhibited efficient mitochondrial respiration (Cooper *et al.*, 2012; Chen *et al.*, 2014), similar to wild-type cells (Supplementary Fig. 2). These results suggest that the *ATAD1* mutation has no significant effect on mitochondrial function, despite reduction in the level of some mitochondrial proteins.

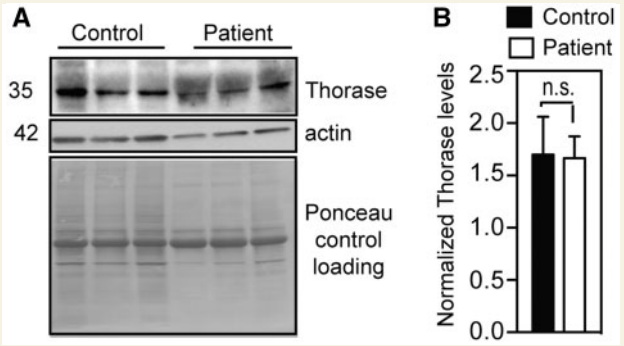

Figure 2 Mutant Thorase is expressed in patient-derived fibroblasts. (**A**) Immunoblot of lysates obtained from patient and control fibroblasts. Expression of Thorase was monitored by using anti-Thorase antibody, and anti-actin antibody was used to control for equal loading. As the anti-Thorase antibody was generated against the C-terminus and this region contains a new amino acid composition in the mutant, detection of Thorase in patient cells was difficult (compare the clear band in control and the diffuse band in patient cells). (**B**) Optical densitometry quantification of **A**. Values represent the mean ± SEM ($n = 3$, n.s. $P > 0.05$, Tukey's multiple comparison tests).

ATAD1 mutation p.(His357Argfs*15) affects the oligomeric state of Thorase but causes no defects in its ATPase activity

The predicted 3D model of Thorase suggests that the *ATAD1* mutation p.(His357Argfs*15) results in changes in the secondary structure at the C-terminus of Thorase (Fig. 3D). The wild-type C-terminus (Ala349-Asp361) is predicted to form a helix, while in the Thorase mutant^{His357Argfs*15} the helix is shortened and sandwiched by two loops to form a loop-helix-loop (LHL) structure (Fig. 3D). To further examine the activity of the Thorase mutant^{His357Argfs*15}, a recombinant expression vector encoding for it was generated. Purified wild-type Thorase elutes as 70 kDa (dimer) on a size-exclusion column, while the mutant^{His357Argfs*15} elutes at a higher molecular weight >400 kDa (Fig. 3E). Thus, the p.(His357Argfs*15) mutation seems to lock the Thorase mutant in an oligomeric state. Both wild-type and mutant migrated at ~36 kDa in SDS-PAGE as indicated by Coomassie staining and immunoblot analysis, however, the mutant migrated higher than the wild-type due to the elongated C-terminus (Fig. 3F). ATP binding assessment using UV light-induced cross-linking (Harvey *et al.*, 2008) of radiolabelled [α-P^{32}]ATP bound to purified recombinant proteins suggested that the Thorase mutant binds ATP similar to wild-type (Supplementary Fig. 2). Similarly, ATP hydrolysis was not significantly affected in the mutant (Supplementary Fig. 2). These results indicate that the p.(His357Argfs*15) mutation does not affect ATPase activity of Thorase but strongly impacts its oligomeric state, most likely as a result of the LHL formation at the C-terminus.

The Thorase mutant^{His357Argfs*15} shows defects in the disassembly of AMPAR-GRIP1 and Thorase oligomer complexes

Since Thorase regulates AMPAR trafficking (Zhang *et al.*, 2011; Prendergast *et al.*, 2014), we examined Thorase mutant^{His357Argfs*15} interactions with GluA2-GRIP1 complex and particularly its disassembly. Purified GST-Thorase wild-type and mutant were immobilized on beads and mixed with Thorase knockout (*Atad1*$^{-/-}$) whole brain lysates in the presence of ADP, ATP or ATPγS (Fig. 4A–D). Both wild-type and mutant bound efficiently to the GluA2-GRIP1 complex in the presence of non-hydrolysable ATPγS, which maintains Thorase in the oligomeric substrate-bound state (Fig. 4A–C). However, in the presence of ATP, which can be hydrolysed and is required for the proper disassembly of protein complexes by Thorase, wild-type Thorase disassembled the complex, whereas the disassembly was significantly impaired by the Thorase mutant^{His357Argfs*15} (Fig. 4D). These data suggest that the p.(His357Argfs*15) mutation affects Thorase-mediated AMPAR trafficking, likely by impairing its transition from oligomeric to monomeric state. The formation of oligomeric complexes by Thorase and other AAA+ ATPases is critical for their proper assembly and disassembly of protein complexes (Fujiki *et al.*, 2008). Therefore, we attempted to determine whether the defect in AMPAR complex disassembly by the mutant^{His357Argfs*15} results from improper Thorase oligomer disassembly. Oligomeric formation and disassembly were evaluated by ATP binding and glutaraldehyde cross-linking of protein complexes (Babst *et al.*, 1998). Purified Thorase samples were mixed with ATP (at 4°C to prevent its hydrolysis or at 37°C to allow for its hydrolysis) or non-hydrolysable ATPγS (Supplementary Fig. 2). In the presence of either ATP at 4°C (ATP-4) or ATPγS Thorase formed large oligomeric complexes of molecular weights greater than 250 kDa (Supplementary Fig. 2). While 71 ± 4.7% of Thorase wild-type formed oligomers, 89 ± 6.3% of the mutants were found in the oligomeric state (ATP-4 in Supplementary Fig. 2). Upon ATP hydrolysis (ATP-37), 75.5 ± 4.4% of Thorase wild-type and 57.6 ± 7.6% of mutant disassembled oligomeric complexes (Supplementary Fig. 2). These results indicate and further confirm that the p.(His357Argfs*15) mutation impairs normal disassembly of Thorase oligomers. Although we observed a defect of 14–18% in oligomeric disassembly in the Thorase mutant^{His357Argfs*15} compared to wild-type, this may be significant enough to cause severe consequences in terms of clinical phenotype.

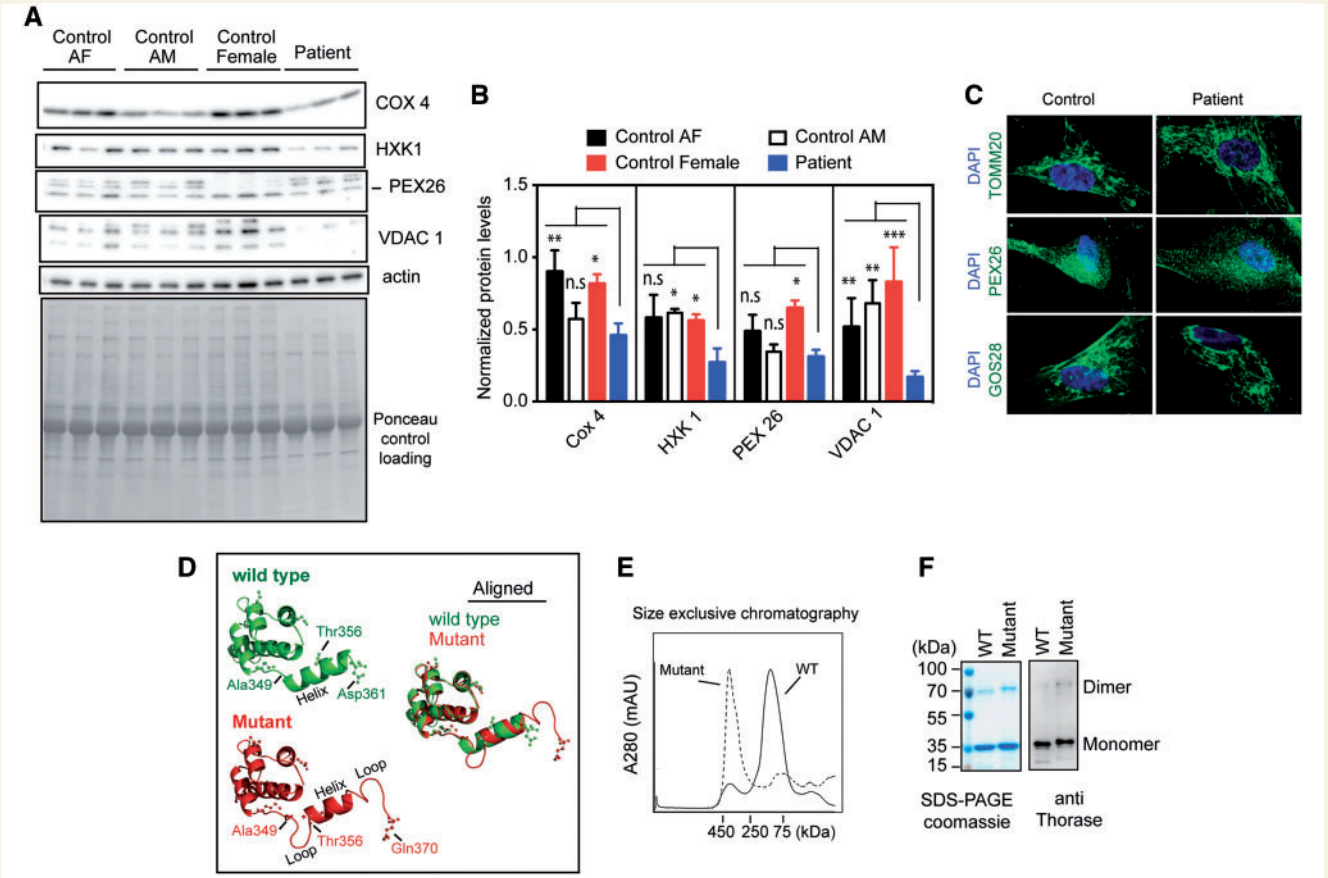

Figure 3 The *ATAD1* mutation p.(His357Argfs*15) leads to reduced amount of some mitochondrial proteins in patient-derived fibroblasts and locks Thorase in the oligomeric state. (**A**) Immunoblots of lysates obtained from patient and control fibroblasts. COX4 = cytochrome *c* oxidase subunit 4; HXK1, = hexokinase 1; PEX26 = peroxisomal biogenesis factor 26; VDAC1 = voltage dependent anion channel 1. (**B**) Optical densitometry quantification of (**A**). Values represent the mean + SEM ($n = 3$, $^{***}P < 0.01$, $^{**}P < 0.05$, $^{*}P < 0.10$, n.s. $>$ 0.10, two-way ANOVA, Tukey's multiple comparison tests). (**C**) Representative immunofluorescence images of the mitochondrial morphology (TOMM20 staining) in control and patient fibroblasts. The cells were also stained for Golgi (GOS28), peroxisomes (PEX26) and the nuclei with DAPI (blue). (**D**) Predicted 3D structure of Thorase wild-type (green) and mutant^{His357Argfs*15} (red). (**E**) Size exclusive chromatograph profile of purified recombinant Thorase. Wild-type Thorase appears as a dimer (~70 kDa), whereas the Thorase mutant^{His357Argfs*15} appears as oligomer ($>$400 kDa). (**F**) Purified proteins resolved on 10% SDS-PAGE stained with coomassie (*left*) and immunoblotted with anti-Thorase antibody (*right*).

Atad1$^{-/-}$ neurons expressing the Thorase mutant^{His357Argfs*15} display reduced GluA2 surface expression

Since Thorase regulates surface expression of AMPARs the effects of the p.(His357Argfs*15) mutation on AMPARs trafficking was evaluated. An antibody-feeding assay for endocytosis of surface GluA2 receptors (Zhang *et al.*, 2011; Prendergast *et al.*, 2014) was performed in *Atad1*$^{-/-}$ primary cortical neurons expressing GFP-tagged Thorase wild-type or mutant^{His357Argfs*15}. Live neurons were incubated with an anti-GluA2 N-terminal antibody followed by induction of GluA2 endocytosis with NMDA (20 μM) and glycine (10 μM). In control unstimulated Thorase mutant^{His357Argfs*15} cultures there was decreased surface expression of GluA2 compared to Thorase wild-type cultures (Fig. 4E and F). In contrast, the ratio of surface GluA2/intracellular GluA2 in NMDA- and glycine-stimulated Thorase mutant cortical cultures remained similar to that of stimulated Thorase wild-type cultures (Fig. 4G and H). Thus, the mutant^{His357Argfs*15}-expressing neurons exhibited significantly reduced surface GluA2 only under unstimulated conditions. To further evaluate the effects of the p.(His357Argfs*15) mutation in Thorase on AMPAR trafficking, GluA2 surface expression was assessed by a bis(sulfosuccinimidyl)-suberate (BS3) cross-linking assay that allows for the quantification of both surface and intracellular receptor pools (Conrad *et al.*, 2008). The results suggested decreased levels of surface GluA2 in unstimulated mutant^{His357Argfs*15}-expressing cultures compared to wild-type-expressing cultures (Fig. 4I and J). In response to NMDA, there was no significant difference in internalization of surface GluA2 in the two cultures (Fig. 4I and J). Together, the data suggest that the Thorase mutant^{His357Argfs*15} may inhibit the recycling back and/or

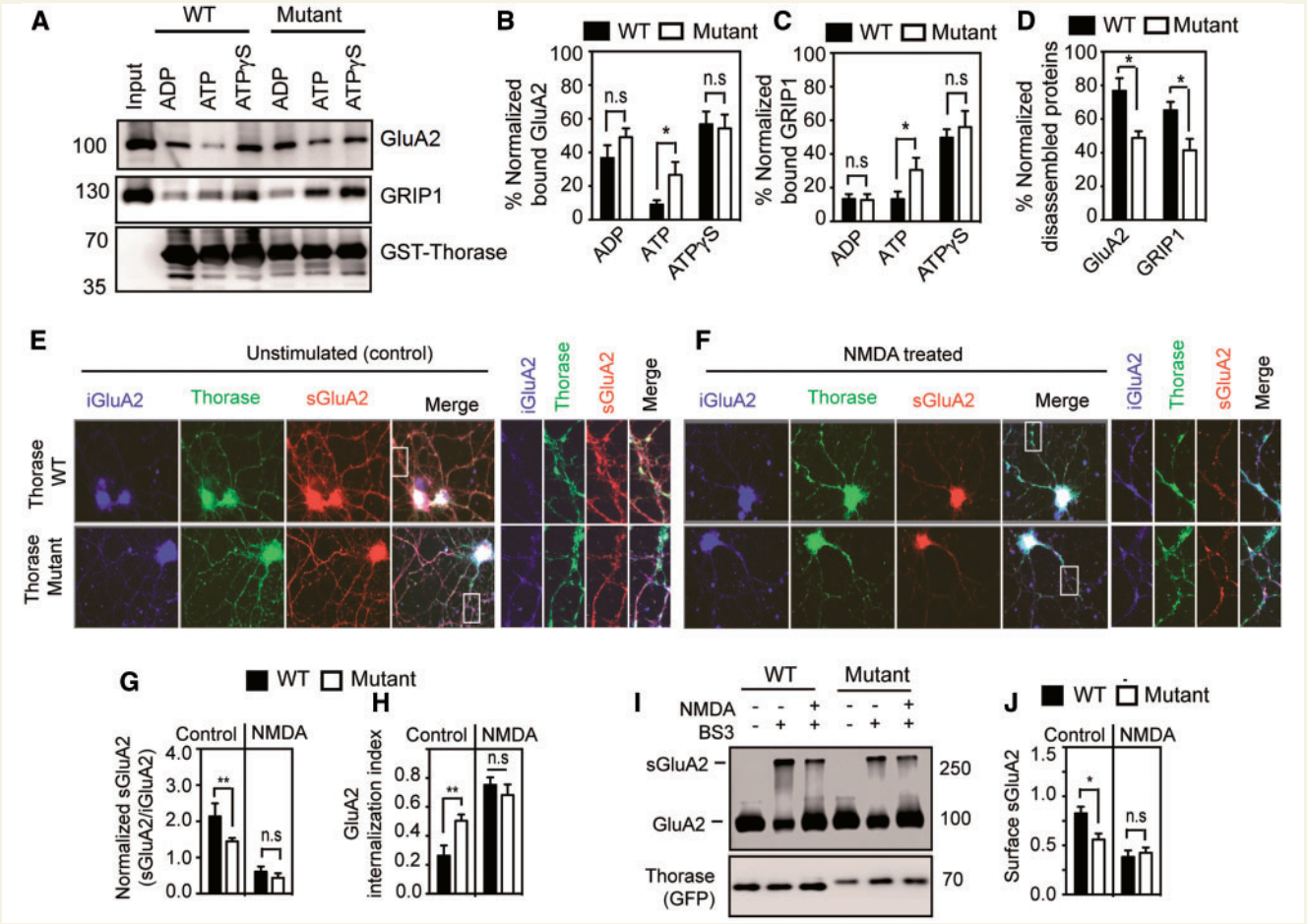

Figure 4 ***ATAD1*** **mutation p.(His357Argfs*15) affects GluA2-GRIP1 complex disassembly and GluA2 surface expression.** (**A**) Immunoblot analyses of GST-Thorase pulldown of the GluA2-GRIP1 complex from Thorase knockout whole brain lysate in the presence of different nucleotides (ATP = hydrolysable ATP; ATPγS = non-hydrolysable ATP). The samples were incubated at 4°C for binding and then at 37°C for ATP hydrolysis to trigger the disassembly of the protein complex. (**B** and **C**) The graphs represent normalized per cent bound GluA2 (**B**) and GRIP1 (**C**) in the GST-Thorase pulldown samples for **A**. (**D**) Normalized percentage of GluA2 and GRIP1 disassembled from Thorase-GluA2-GRIP1 complex in **A**. (**E** and **F**) Representative immunofluorescence images of unstimulated and NMDA-induced endocytosis of GluA2 in *Atad1*$^{-/-}$ neurons expressing Thorase-GFP wild-type (WT) or the mutant^{His357Argfs*15} (Mutant). (**G**) Normalized ratio of surface GluA2 (sGluA2) to internalized GluA2 (iGluA2) for **E** and **F**. (**H**) GluA2 internalization index measured as the ratio of iGluA2 to the total GluA2 (iGluA2 plus sGluA2) fluorescence intensities. (**I**) Immunoblot analyses of BS3-crosslinking of sGluA2 in *Atad1*$^{-/-}$ neurons expressing Thorase-GFP wild-type or mutant^{His357Argfs*15}. (**J**) The normalized optical densitometry quantification of sGluA2 for **I**. Mean ± SEM of three experiments performed in triplicate. $n = 3$, $^{**}P < 0.05$, $^{*}P < 0.10$, n.s. $P > 0.10$, ANOVA with Tukey-Kramer *post hoc* test when compared with wild-type.

reinsertion of AMPARs to the surface following endocytosis resulting in a decrease in the steady-state levels of these receptors at the cell surface.

Discussion

ATAD1 encodes Thorase, which is highly expressed in mouse brain and testis (Zhang *et al.*, 2011). Members of the AAA+ superfamily of ATPases are involved in the unfolding of proteins and disassembly of protein complexes and aggregates (Hanson and Whiteheart, 2005). In addition, Thorase is able to maintain mitochondrial function through degradation of mislocalized tail-anchored proteins to the outer mitochondrial membrane, thus playing an important role in maintenance of mitochondrial function and integrity (Chen *et al.*, 2014; Okreglak and Walter, 2014). A similar caretaker function of Thorase has also been proposed for peroxisomes (Grimm *et al.*, 2016). In addition, postsynaptically, Thorase controls the internalization of excitatory, glutamatergic AMPARs by disassembling complexes between glutamate receptor interacting protein (GRIP1) and the AMPAR subunit GluA2. Therefore, Thorase deficiency is expected to impair function of mitochondria and peroxisomes and alter neurotransmission. Accordingly, Thorase deficiency in mice leads to enhanced AMPAR density at the cell surface that results in enhanced excitatory postsynaptic currents and impaired adaption to excitatory stimuli. Although homozygous *Atad1* knockout mice are viable and do not

show any obvious gross malformation, approximately 80% die of a seizure-like syndrome (Zhang *et al.*, 2011). The C-terminus of Thorase is evolutionarily highly conserved (Supplementary Fig. 1) and involved in intra- and intermolecular contacts of oligomerized AAA+ ATPase complexes (Grimm *et al.*, 2016). The *ATAD1* mutation identified here causes a deletion of the last five residues of the C-terminus with addition of 14 novel amino acids (Fig. 1C and Supplementary Fig. 1).

Our results demonstrate that a homozygous frameshift mutation at the 3′ end of *ATAD1* leads to the production of Thorase protein with a novel function of its C-terminal end. Interestingly, through a gain-of-function effect, an unusual mechanism in autosomal recessive disease, the *ATAD1* mutation causes a congenital severe and lethal encephalopathy associated with stiffness and arthrogryposis. Previously, we reported a homozygous loss-of-function mutation (p.Glu276*) in *ATAD1* that underlies a neurological disorder with remarkable clinical overlap to the phenotype reported here: patients showed hypertonia, seizures, respiratory failure and early death (Ahrens-Nicklas *et al.*, 2017). In the affected neonates, movement was precluded due to extreme hypertonia. Thus, stiffness was common to both families [this report and Ahrens-Nicklas *et al.* (2017)], while clinical seizures starting at birth were only present in infants with *ATAD1* nonsense mutation (Ahrens-Nicklas *et al.*, 2017). Given that different *ATAD1* mutations have been identified in two separate families with critical neurological phenotypes in neonates, *ATAD1* can be considered as an important human disease gene. Our functional assays showed deficiency in AMPAR recycling as the molecular mechanism associated with the disease. The gain-of-function mutation in *ATAD1* decreases the population of excitatory postsynaptic AMPA receptors. However, mitochondrial function does not seem to be affected by the *ATAD1* p.(His357Argfs*15) mutation as patient-derived fibroblasts show normal mitochondrial morphology and respiratory chain performance. In contrast, *Atad1* loss-of-function causes a decrease of many mitochondrial proteins in mouse brain in which the Golgi protein GOS28 ectopically accumulated. In addition, *Atad1*-deficient mouse embryonic fibroblasts show decreased basal and mitochondrial respiration, severely fragmented mitochondria and mislocalization of GOS28 and PEX26 in mitochondria suggesting significant mitochondrial impairment in this mouse mutant (Chen *et al.*, 2014). These findings together with impaired AMPAR internalization resulting in increased GluA1 and GluA2 surface levels in *Atad1* knockout neurons suggest a combined effect of defects in both AMPAR trafficking and mitochondrial function that might have contributed to the phenotype in *Atad1*$^{-/-}$ mice (Zhang *et al.*, 2011; Chen *et al.*, 2014). Similarly, we speculate that the distinct combination of functional alterations arising from either gain- or loss-of-function *ATAD1* mutations may provide an explanation for the discrete although overlapping phenotypes observed in the siblings reported here and the previously described family (Ahrens-Nicklas *et al.*, 2017).

Changes in AMPAR surface expression is a known pathogenic mechanism in encephalopathy; for example, a decrease in extrasynaptic AMPAR expression impairs synaptic plasticity in a model of hepatic encephalopathy (Schroeter *et al.*, 2015). This disrupts the efficacy of synaptic transmission and the fine balance between inhibitory and excitatory signalling, which accounts, at least partially, for the encephalopathy. There are additional possible targets of Thorase that contribute to the encephalopathy and neurologic phenotype of patients with mutations in *ATAD1*. Consistent with this notion is the observation that the AMPAR antagonist, perampanel, only partially rescued the phenotype of patients with a loss-of-function mutation in *ATAD1* (Ahrens-Nicklas *et al.*, 2017). The findings from our study establish an important avenue for clinicians to examine the role of *ATAD1* mutations in several neurological diseases due to unknown cause.

Acknowledgements

We thank the family for their support.

Funding

This work was supported by a grant from the Deutsche Forschungsgemeinschaft (KU 1240/10-1 to K.K.) and National Institutes of Health – National Institute on Drug Abuse, P50DA000266 to V.L.D and T.M.D.

Supplementary material

Supplementary material is available at *Brain* online.

References

Ahrens-Nicklas RC, Umanah GK, Sondheimer N, Deardorff MA, Wilkens AB, Conlin LK, et al. Precision therapy for a new disorder of AMPA receptor recycling due to mutations in ATAD1. Neurol Genet 2017; 3: e130.

Arnold K, Bordoli L, Kopp J, Schwede T. The SWISS-MODEL workspace: a web-based environment for protein structure homology modelling. Bioinformatics 2006; 22: 195–201.

Babst M, Wendland B, Estepa EJ, Emr SD. The Vps4p AAA ATPase regulates membrane association of a Vps protein complex required for normal endosome function. EMBO J 1998; 17: 2982–93.

Bolger AM, Lohse M, Usadel B. Trimmomatic: a flexible trimmer for Illumina sequence data. Bioinformatics 2014; 30: 2114–20.

Carta E, Chung SK, James VM, Robinson A, Gill JL, Remy N, et al. Mutations in the GlyT2 gene (SLC6A5) are a second major cause of startle disease. J Biol Chem 2012; 287: 28975–85.

Cartault F, Munier P, Benko E, Desguerre I, Hanein S, Boddaert N, et al. Mutation in a primate-conserved retrotransposon reveals a noncoding RNA as a mediator of infantile encephalopathy. Proc Natl Acad Sci USA 2012; 109: 4980–5.

Chen YC, Umanah GK, Dephoure N, Andrabi SA, Gygi SP, Dawson TM, et al. Msp1/ATAD1 maintains mitochondrial function by facilitating the degradation of mislocalized tail-anchored proteins. EMBO J 2014; 33: 1548–64.

Conrad KL, Tseng KY, Uejima JL, Reimers JM, Heng LJ, Shaham Y, et al. Formation of accumbens GluR2-lacking AMPA receptors mediates incubation of cocaine craving. Nature 2008; 454: 118–21.

Cooper O, Seo H, Andrabi S, Guardia-Laguarta C, Graziotto J, Sundberg M, et al. Pharmacological rescue of mitochondrial deficits in iPSC-derived neural cells from patients with familial Parkinson's disease. Sci Transl Med 2012; 4: 141ra90.

Fujiki Y, Miyata N, Matsumoto N, Tamura S. Dynamic and functional assembly of the AAA peroxins, Pex1p and Pex6p, and their membrane receptor Pex26p involved in shuttling of the PTS1 receptor Pex5p in peroxisome biogenesis. Biochem Soc Trans 2008; 36: 109–13.

Grimm I, Erdmann R, Girzalsky W. Role of AAA(+)-proteins in peroxisome biogenesis and function. Biochim Biophys Acta 2016; 1863: 828–37.

Hanson PI, Whiteheart SW. AAA+ proteins: have engine, will work. Nat Rev Mol Cell Biol 2005; 6: 519–29.

Harvey RJ, Topf M, Harvey K, Rees MI. The genetics of hyperekplexia: more than startle! Trends Genet 2008; 24: 439–47.

Kelley LA, Mezulis S, Yates CM, Wass MN, Sternberg MJ. The Phyre2 web portal for protein modeling, prediction and analysis. Nat Protoc 2015; 10: 845–58.

Kevelam SH, Bugiani M, Salomons GS, Feigenbaum A, Blaser S, Prasad C, et al. Exome sequencing reveals mutated SLC19A3 in patients with an early-infantile, lethal encephalopathy. Brain 2013; 136: 1534–43.

Koch MC, Ricker K, Otto M, Grimm T, Bender K, Zoll B, et al. Linkage data suggesting allelic heterogeneity for paramyotonia-congenita and hyperkalemic periodic paralysis on chromosome-17. Hum Genet 1991; 88: 71–4.

Kortüm F, Caputo V, Bauer CK, Stella L, Ciolfi A, Alawi M, et al. Mutations in KCNH1 and ATP6V1B2 cause Zimmermann-Laband syndrome. Nat Genet 2015; 47: 661–7.

Okreglak V, Walter P. The conserved AAA-ATPase Msp1 confers organelle specificity to tail-anchored proteins. Proc Natl Acad Sci USA 2014; 111: 8019–24.

Prendergast J, Umanah GK, Yoo SW, Lagerlof O, Motari MG, Cole RN, et al. Ganglioside regulation of AMPA receptor trafficking. J Neurosci 2014; 34: 13246–58.

Schroeter A, Wen S, Molders A, Erlenhardt N, Stein V, Klocker N. Depletion of the AMPAR reserve pool impairs synaptic plasticity in a model of hepatic encephalopathy. Mol Cell Neurosci 2015; 68: 331–9.

Seelow D, Schuelke M, Hildebrandt F, Nurnberg P. HomozygosityMapper–an interactive approach to homozygosity mapping. Nucleic Acids Res 2009; 37: W593–9.

Tijssen MAJ, Rees MI. Hyperekplexia. In: Pagon RA, Adam MP, Ardinger HH, Wallace SE, Amemiya A, Bean LJH, et al., editors. GeneReviews(R) Seattle (WA): University of Washington; 1993.

Zhang J, Wang Y, Chi Z, Keuss MJ, Pai YM, Kang HC, et al. The AAA+ ATPase Thorase regulates AMPA receptor-dependent synaptic plasticity and behavior. Cell 2011; 145: 284–99.